

1 A novel technique for interface analysis: behaviour of
2 sophorolipids biosurfactant obtained from *Meyerozyma*
3 spp. MF138126 during low-salinity heavy-crude
4 experiments

5 Lateef T. Akanji¹ and Ramla Rehman² and Chibuzo C. Onyemara¹ and
6 Rainer Ebel³ and Asif Jamal²

7 ¹ *Division of Petroleum Engineering, School of Engineering, University of Aberdeen,*
8 *Aberdeen AB24 3FX, UK*

9 ² *Department of Microbiology, Faculty of Biological Sciences, Quaid-i-Azam*
10 *University, Islamabad- 45320, Pakistan*

11 ³ *School of Natural and Computing Sciences, University of Aberdeen, Aberdeen, UK,*
12 *AB24 3FX*

13 **Abstract**

14 A novel technique for interface behaviour and thermodynamic properties
15 analyses of sophorolipids (SLs) biosurfactant obtained from *Meyerozyma* spp.
16 MF138126 under high-pressure high-temperature (HPHT), for low-salinity
17 heavy-crude experiments is presented. An experimental rig for production
18 of biosurfactant and determination of interfacial tension (IFT) under HPHT
19 is developed specially for the purpose of this investigation. A reduction of
20 a factor of seven and nine in IFT was obtained for experiments between
21 brine and heavy-crude at temperatures of 45°C and 65°C respectively. Fur-
22 thermore, with increasing temperature, the degree of SLs adsorption at the
23 interface increases leading to a total collapse in the profiles of the adsorption
24 graphs. The minimum area per molecule of SLs monomers for different con-
25 ditions suggested that the interface weakens occupying more surface area as
26 the temperature increases. The degree of counter-ion binding for SLs is ob-
27 tained to be 0.86. The computed Gibbs free energy of micellisation is -1940
28 KJ/mol; which is exergonic depicting favourable reaction and spontaneous
29 in forward direction. At a fixed temperature of 25°C and pressure of 45 bar,
30 IFT value of 0.251 mN/m was obtained. It is concluded that the produced
31 SLs retained its molecular integrity and IFT reduction effectiveness under

32 both unconfined and confined HPHT systems.

33 *Keywords:* Interfacial phenomenon,, HPHT, Anaerobic fermentation,
34 Microbial EOR, Biosurfactant producing microbes, High-temperature
35 cultivation, Low-salinity, Heavy-crude

36 1. Introduction

37 Enhanced Oil recovery (EOR) is a tertiary method that improves the
38 recovery of petroleum hydrocarbons from the reservoir after primary and
39 secondary production phases. In recent years, variety of methods like ther-
40 mal, chemical and miscible or solvent injection which involve the use of steam,
41 surface active compounds and hydrocarbon gases, respectively, have been em-
42 ployed for EOR. Amongst the different types of surface active compounds,
43 cationic and anionic surfactants are known to possess positively and nega-
44 tively charged ions respectively; while amphoteric surfactants possess both
45 positively and negatively charged ions (Tadros [1]). The amphiphilic nature
46 of surfactants make them readily able to dissociate in polar and non-polar
47 fluids (Koh et al. [2], Bollmann et al. [3], Wang et al. [4]). However, due to
48 the environmental risks associated with the use of chemical surfactants and
49 the possible high expenses, there is a need to develop alternative methods
50 that are environmentally benign and also capable of enhancing oil recovery
51 (e.g. Kiran et al. [5], Ramos et al. [6]). The surfactant solution will dissoci-
52 ate to form monomers at the initial stage, while the dissociated monomers
53 will later aggregate at increasing concentration to form micelles commonly
54 referred to as supramolecules (Desai and Banat [7]).

55
56 Microbial EOR (MEOR) encompasses the use of microorganisms and
57 their products to extract the remaining oil from reservoirs. Further, due to its
58 green nature and eco-friendliness, MEOR is gaining considerable importance
59 as it provides biotechnological solution to the problems of the petroleum in-
60 dustry (e.g. Al-Sulaimani et al. [8] Chisholm et al. [9], Budiharjo et al. [10]).
61 MEOR can be achieved either by insitu injection of microorganisms or by
62 the mass flooding of nutrients, biosurfactants, biopolymers, biologically pro-
63 duced acids, gases and solvents into the reservoir (e.g. Poremba et al. [11]).
64 We advocate ex-situ production of biosurfactant where interfacial adsorption
65 and thermodynamic properties are critically evaluated prior to utilisation.
66 The thermodynamic standard Gibbs free energy required for the formation

67 of SLs; a type of glycolipids obtained from the strain of *Meyerozyma*, which
68 can be used in the prediction of the degree of spontaneity, surface adsorption,
69 surface affinity and binding potentials, critical micelle concentration (CMC)
70 aggregates formation in immiscible bulk water phase and rapid surface ten-
71 sion (ST) and IFT reduction property has never been studied or published
72 to the best of our knowledge.

73

74 The mechanisms associated with adsorption of biosurfactants at the in-
75 terfaces involve ion exchange where previously adsorbed counterions at the
76 interface are replaced by similar but different ions from the bulk solution;
77 ion-pairing in which surfactants are adsorbed on to free counterions from the
78 solution; hydrogen bonding and Van der Waal dispersive forces (Norde [12],
79 Nakanishi et al. [13], Rosen [14]). Previous studies have demonstrated the
80 application of some biosurfactants producing microorganisms in EOR related
81 studies. This is mainly related to their ability to reduce the oil-water IFT
82 (e.g. Al-Wahaibi et al. [15], Al-Araji et al. [16], Anitha and Jeyanthi [17]).
83 However, adsorption of sophorolipids (SLs) at heavy crude oil-brine interface
84 has not been established (Speight [18] and Lanier [19]). Most studies on
85 adsorption of some other biosurfactants have been in medical, food sciences
86 and environmental remediation (Keomany and Asnachinda [20]).

87

88 Recently, some researchers have isolated yeast for the production of bio-
89 surfactant purposes. For instance, Camargo et al. [21] characterised and
90 evaluated the capacity of yeast to produce biosurfactant under acidic condi-
91 tions using soybean oil frying waste as the main source of carbon. Specific
92 application was in bioremediation and metal removal processes in anaero-
93 bic sewage sludge. Under a similar application, Camargo et al. [22] inves-
94 tigated the influence of co-inoculation of *Acidithiobacillus* bacteria and the
95 biosurfactant-producing yeast *Meyerozyma guilliermondii* in bioleaching pro-
96 cesses. This study suggested that after 10 days of incubation, 76.5% of Zn,
97 59.8% of Ni, 22.0% of Cu, 9.8% of Cd, 9.8% Cr and 7.1% of Pb were solu-
98 bilised with the presence of yeast contributing to the reduction in the time
99 required for Cd to solubilise from 240 to 96 h.

100

101 Despite the recent advances in the production of biosurfactant from yeasts,
102 application has only been limited to ambient conditions of low-pressure low-
103 temperature (e.g. Liang et al. [23]) associated with environmental remedi-
104 ation processes. Ganji et al. [24] reported the production of sophorolipids

105 from an isolated strain of *Candida keroseneae* under ambient condition and
106 its possible use in MEOR. In another study, Elshafie et al. [25] conducted
107 core flooding experiments using the SLs produced from a strain of *Candida*
108 *bombicola*. For this purpose, the seed culture was incubated at room tem-
109 perature. However, specific application in MEOR process under elevated
110 insitu conditions is sparse. Further, microorganisms isolated for MEOR
111 should endure high temperature, pressure and salinity and be capable of
112 growth under anaerobic or microaerophilic conditions. Up till now, differ-
113 ent strains of *Bacillus*, *Geobacillus*, *Pseudomonas*, *Rhodococcus*, *Clostridium*,
114 *Mycobacterium* and *Brevibacterium* have been used in various in-situ MEOR
115 studies. However, the mechanisms underpinning the full spectrum of anaer-
116 obic fermentation, high-pressure high-temperature (HPHT) anaerobic cul-
117 tivation, screening, physico-chemical analysis of SLs biosurfactant obtained
118 from *Meyerozyma* spp. MF138126; prior to EOR applications, have not been
119 previously investigated and are therefore not well understood.

120

121 One aspect of this work therefore involves development of a novel tech-
122 nique for the production of SLs biosurfactant under HPHT conditions on
123 the one hand and evaluation of the interface behaviour of the produced SLs
124 during low-salinity heavy-crude experiments on the other hand. The other
125 aspect involves the development of an unconventional technique for interface
126 analysis under HPHT insitu conditions. Conventional techniques involve cou-
127 pling an image analysis package using video camera, data acquisition system
128 and commercial algorithms for the measurement of the coordinates of the
129 pendant drop to determine IFT or ST (e.g. Bagalkot et al. [26]). In this
130 unconventional design setup, the IFT chamber has a design pressure and
131 temperature of 500 MPa (5000 bar) and 175 °C respectively. Furthermore,
132 the system also allows for both bubble and pendant drop experimental mea-
133 surements to be carried in a single setup.

134

135 The potential of the newly isolated SLs producing microbial strain of
136 *Meyerozyma* spp. MF138126 to increase recovery of heavy crude oil through
137 surface and IFT reduction in a typical low formation salinity water is there-
138 fore investigated. In order to achieve this, a novel protocol for cultivation
139 of previously optimised strains of *Meyerozyma* spp. MF138126 under ele-
140 vated culture temperature and pressure is developed. It involves anaerobic
141 fermentation under shake-flask experiments and then HPHT cultivation for
142 the production of SLs from optimised *Meyerozyma* spp. MF138126. Sam-

143 ples are collected periodically under varying conditions of temperature and
144 pressure to monitor growth-rate and produced cellular biomass using spec-
145 trophotometer. SLs is obtained through solvent extraction technique and
146 the effect of HPHT conditions on their chemical structure was determined
147 through Fourier-transform infrared spectroscopy (FTIR) analysis.

148

149 The economics of the application of SLs biosurfactant can be evaluated as
150 part of crude oil/brine/biosurfactant/rock (COBBIOR) experimental analy-
151 sis. In order to achieve a cost-effective EOR process, biosurfactant affinity
152 to rock surface must be evaluated. Some of the critical COBR parameters
153 include adsorption, precipitation and phase trapping. These parameters have
154 a direct bearing on the porous system temperature and salinity. A significant
155 loss of surfactant may occur due to adsorption of biosurfactant on to the rock
156 surfaces (e.g. Amirianshoja et al. [27] and Barati-Harooni et al. [28]). This
157 may impact the overall cost of the process as well as the effectiveness of the
158 surfactant in reducing IFT.

159

160 In this work, a series of crude oil/brine/biosurfactant (COBBIO) screen-
161 ing experiments involving ST and IFT measurements between typical forma-
162 tion brine and heavy-crude oil in unconfined and confined special purpose
163 HPHT experimental rig is conducted. Adsorption is investigated as part of
164 COBBIO IFT analyses. The thermodynamic behaviour of the SLs is further
165 investigated as outlined in this paper where the tendency for SLs to maintain
166 its structural integrity under reservoir brine system is also established. All
167 data label prefixed by S can be found in the supplementary material. Ap-
168 plication of the produced biosurfactant in actual core-flooding or COBBIOR
169 experiment is outside the scope of this paper.

170 2. Materials and method

171 The new protocol developed for the purpose of this investigation is shown
172 in Fig. 1. It consists of six (6) steps involving: (a) Anaerobic shake-flask
173 cultivation of *Meyerozyma* spp. MF138126 under ambient pressure and tem-
174 perature; (b) Anaerobic cultivation of *Meyerozyma* spp. MF138126 under
175 HPHT by upgrading the shake-flasks cultivation; (c) Spectrophotometric
176 analysis of the microbial growth rate at the two incubation temperatures
177 i.e. 25 and 45 °C, provided in the reactor chamber (d) FTIR spectroscopic
178 analysis of the SLs produced under HPHT conditions; (e) SLs in ST/IFT

179 reduction experiments; (f) SLs in core displacement experiments for possible
 180 role in EOR. Each step involved in the protocol is explained further below.
 181 Step (f) is beyond the scope of this investigation.

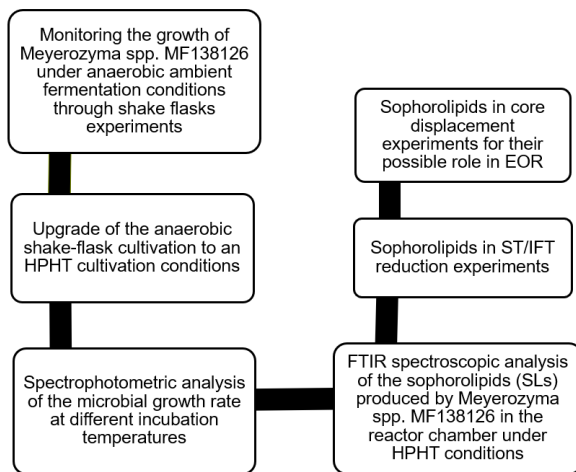


Figure 1: Developed protocol for the microbial enhanced oil recovery process.

182 *2.1. Anaerobic cultivation of Meyerozyma spp. MF138126 under ambient*
 183 *conditions*

184 The strain *Meyerozyma* spp. MF138126 was previously isolated from a
 185 crude oil contaminated site. It was then screened based on its morphological
 186 and molecular identity and screened in order to determine its SLs producing
 187 capabilities (Rehman et al. [29]). Anaerobic cultivation of the strain was
 188 done at lab-scale for a period of one week in a minimal salt medium (MSM)
 189 with the composition highlighted in Table 1. This was followed by the incu-
 190 bation of culture broth in 250 ml Erlenmeyer flasks at 37 °C and atmospheric
 191 pressure. Samples were taken from the culture flasks after every 24 h and the
 192 growth rate was monitored at 600 nm using a UV-visible spectrophotometer.
 193 All readings were taken in triplicates.

194 *2.2. Anaerobic cultivation of Meyerozyma spp. MF138126 under HPHT con-*
 195 *ditions*

196 Anaerobic cultivation of *Meyerozyma* spp. MF138126 was done under
 197 HPHT conditions. The HPHT anaerobic cultivation reactor (Fig. 2) allows a

Table 1: Minimal salt medium (MSM) optimised for the production of sophorolipids from *Meyerozyma* sp. MF138126.

Media Formulation	Quantity (g/L) or (%)	Unit
Glycerol	5	%
NaH ₂ PO ₄	0.4	g/L
Peptone	10	g/L
Yeast Extract	0.5	g/L
MgSO ₄	0.1	g/L

198 wide range of microbial fermentation processes to be carried-out under differ-
 199 ent pressure (designed to operate up to 200 bar) and temperature conditions
 200 (designed to operate up to 250 °C). The salient feature of this advanced rig in-
 201 cludes source of imposed system pressure, automatic vent-gas system, digital
 202 pressure transducer, digital temperature monitoring system, pressure-relief
 203 valve, rupture disc and vent bio-gases storage tank with pressure indicator.
 204 The system is specially configured to allow all produced bio-gases by the
 205 microorganisms to be captured and discharged in a pressure vessel.

206

207 Following the inoculation process, 800 ml of the culture broth was in-
 208 cubated in the reactor chamber of the rig. A pressure of 1 and 10 bar was
 209 supplied to the microbial culture at 25 °C for a period of 7 days in a sequential
 210 experiment. In the last phase of experiment, the temperature was elevated
 211 to 45 °C with the pressure kept constant. Samples were collected at periodic
 212 intervals with a syringe through a three-way check-valve. Growth rate was
 213 monitored by measuring the optical density of culture medium at 600 nm
 214 using a UV-visible spectrophotometer. All readings were taken in triplicates.
 215 Extraction of SLs is then carried out using solvents (Ethyl acetate, Methanol
 216 etc) and chemical/molecular characterisation of SLs through different ana-
 217 lytical techniques; such as Fourier-transform infrared spectroscopy (FTIR)
 218 and liquid chromatography mass-spectroscopy (LCMS) conducted.

219 2.3. FTIR spectroscopic analysis of the SLs produced under HPHT conditions

220 Post incubation at 25 and 45 °C, the culture broth was centrifuged at
 221 10,000 rpm for 10 minutes to remove cell pellet. This was followed by the
 222 structural analysis of sophorolipids produced by *Meyerozyma* spp. MF138126
 223 at the two incubation temperatures through FTIR spectroscopy.

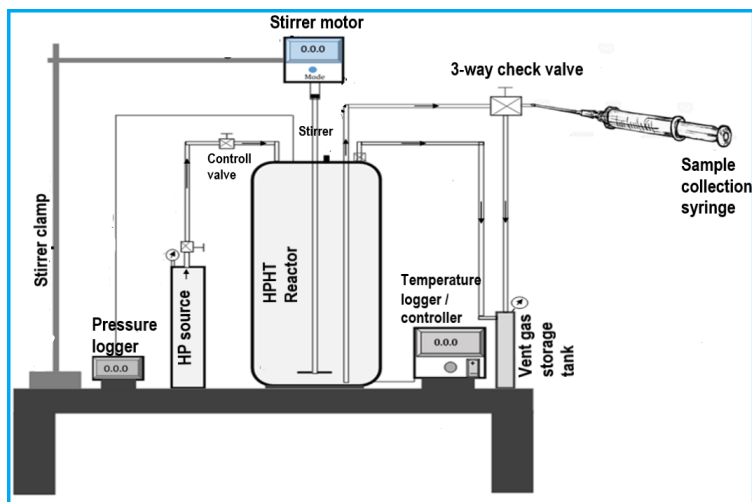


Figure 2: HPHT reactor cell for the anaerobic cultivation of microbes. The features of this advanced rig includes source of imposed system pressure, automatic vent-gas system, digital pressure transducer, digital temperature monitoring system, pressure-relief valve, rupture disc and vent bio-gases storage tank with pressure indicator. Further details on the actual design of the system are available in another publication (Onyemara et al. [30]).

224 *2.4. Principle of IFT measurement*

225 The pendant drop technique is a reliable and an effective method of measuring the IFT of liquid-gas or liquid-liquid system. The shape of the pendant drop (see Fig. 3) is governed by gravity and the ST/IFT (Hansen [31]).
 227 The IFT is calculated from the shadow of the digital image captured by the video-camera using the drop shape analysis which relies on Young-Laplace
 228 equation:
 229
 230

$$\Delta P = \gamma \cdot \left(\frac{1}{r_1} + \frac{1}{r_2} \right), \quad (1)$$

231 where, ΔP is the pressure across the interface, r_1 and r_2 are the principal
 232 radii of the pendant drop, and γ is the ST/IFT.

$$\gamma = \frac{\Delta \rho g R_0^2}{\beta}, \quad (2)$$

233 where, $\Delta \rho$ is the mass density difference between the drop and the surrounding medium, g is the gravity constant, R_0 is the radius of curvature at
 234

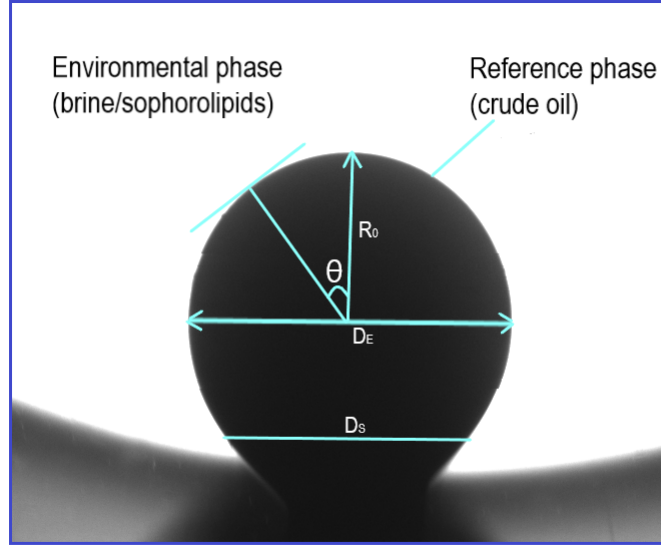


Figure 3: Drop image formed by the reference phase (heavy-crude) in the environmental phase (brine/sophorolipids aqueous solution).

235 the drop apex and β is the shape factor. By convention, $\Delta\rho$ is defined such
 236 that $\Delta\rho$ and β are negative for pendant drops and positive for sessile drops.
 237 For drops that are sufficiently long in order to measure the diameter D_S (i.e.
 238 pendant drops) the maximum diameter, D_E , and the ratio:

$$\nu = \frac{D_S}{D_E}. \quad (3)$$

239 β is then defined thus (see Hansen [31]):

$$\beta = -0.12836 + 0.7577\nu - 1.7713\nu^2 + 0.5426\nu^3 \quad (4)$$

$$\gamma = \frac{\Delta\rho g H^2}{B}, \quad (5)$$

240 where, B is a transformed shape parameter which may be derived from
 241 equations 2 and 5 thus:

$$B = \beta \times \chi^2, \quad (6)$$

242 where, $\chi = \left(\frac{H}{R_0}\right)$, H is the drop height and R_0 is the radius of curvature
243 at the drop apex. From equations 1 - 6 above, it can be observed that with
244 the exception of $\Delta\rho$, the size parameters R_0 and β are derived from the drop
245 profile.

246 2.5. Application of SLs produced by *Meyerozyma* spp. MF138126 in ST and 247 IFT analysis

248 In order to evaluate the effectiveness of the SLs (produced at the two
249 incubation temperatures of 25 and 45 °C) in reducing ST and IFT, sev-
250 eral measurements involving low-pressure low-temperature and low-pressure
251 high-temperature were carried out. Furthermore, the role of crude SLs in
252 interfacial phenomena was determined through special purpose rig assembly
253 involving pendant drop method.

254 2.5.1. ST and IFT reduction analyses for brine and heavy crude oil system 255 (unconfined measurements)

256 In order to measure the ST and IFT of the liquid-liquid and liquid-air
257 phases, a Kruss K-6 tensiometer was used. First, the kit was calibrated
258 with deionised water by taking surface-to-air measurements in triplicate to
259 obtain an average reading of 72.2 dynes/cm (e.g. Heller et al. [32]). The
260 surface activity of the SLs produced by *Meyerozyma* spp. MF138126 was
261 then determined by making separate dilutions of the two supernatants ob-
262 tained at 25 °C and 45 °C in a typical formation brine (composition in Table
263 2). Thereafter, a thin film of heavy crude oil was added onto the surface to
264 create biosurfactant-brine and heavy crude oil interface. ST and IFT mea-
265 surements of the samples were recorded at three different temperatures of
266 25, 45 and 65 °C. Briefly, a platinum ring is lowered into each of the solu-
267 tions to be analysed until it is completely submerged. Upon pulling the ring
268 vertically upward and out of the sample solution, the force that is required
269 to ultimately break contact of the ring to the solution is measured.

270

271 Fig. 4 shows the dynamic viscosity profile as a function of temperature
272 for the heavy crude oil system used in this investigation. Measurements were
273 carried out by measuring dynamic viscosity and generating a profile created
274 by cooling the sample from 80° down to as low as readings could be measured,
275 using the Brookfield method (Intertek UK). For this sample, it is evident that
276 the viscosity increases dramatically at around 40° and basically indicating

277 why it was not possible to take measurements at 30° and below.

278

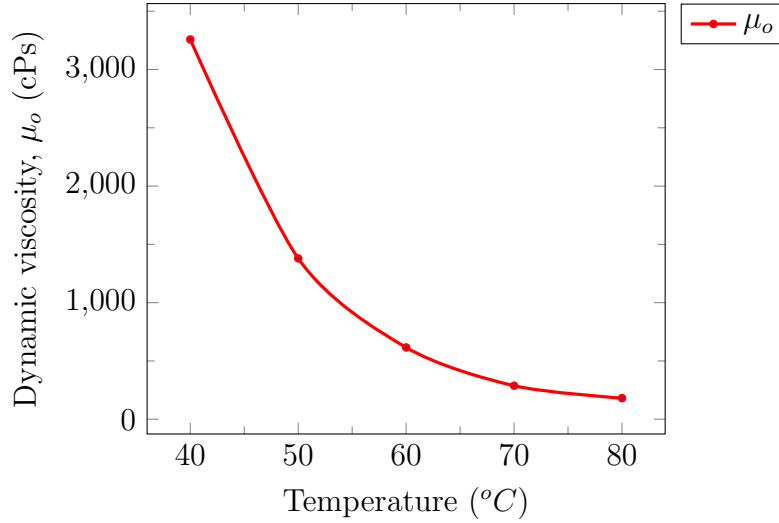


Figure 4: Dynamic viscosity profile as a function of temperature for the heavy crude oil system used in this investigation.

Table 2: Typical low-salinity formation brine formulated and used in this investigation.

Material	Mass (mg)	Deionised water volume (ml)	Material MW (mg/mol)	Molarity (mg/l)
Sodium chloride (NaCl)	23740		58440	0.40623
Potassium chloride (KCl)	755.0		74551.3	0.01013
Magnesium chloride hexahydrate (MgCl ₂ .6H ₂ O)	10700		203310	0.05263
Calcium chloride dihydrate (CaCl ₂ .2H ₂ O)	1500	1000	147008	0.01020
Strontium chloride hexahydrate (SrCl ₂ .6H ₂ O)	24.00		266620	0.00009
Sodium sulfate (Na ₂ SO ₄)	3976		142040	0.02799
Sodium bicarbonate (NaHCO ₃)	194.0		84007	0.00231
Total dissolved solid (TDS) and brine stock molarity	40889			0.50958

Stock brine pH: 7.51

279 2.5.2. HPHT IFT experimental set-up

280 Fig. 5 shows the schematics of the special purpose HPHT IFT experimen-
 281 tal set-up specially developed for the purpose of this investigation. The main

282 component part of the set-up is the HPHT pendant drop chamber built by
283 Sitec-Sieber Engineering and re-designed and re-fabricated in-house to mea-
284 sure the system IFT under varying experimental pressure and temperature.
285 The design pressure and temperature are 500 MPa (5000 bar) and 175 °C
286 respectively. The chamber also has a unique customised dual-drop needle
287 that allows for a phase to be dropped from the roof capillary-needle (for
288 $\rho_d > \rho_e$) or from the bottom capillary-needle (for $\rho_d < \rho_e$) respectively. The
289 HPHT chamber has two see-through windows coupled with a fixed Rame-
290 Hart video-camera/frame grabber combination on one side and and a light
291 source (illuminator) on the other side (see Fig. 5). The video-camera is
292 placed at a distance of 0.049 m (49 mm) from the fore-ground see-through
293 window and the aspect ratio adjusted by calibration both in vertical and
294 horizontal direction. The light source is tilted at an angle of 50 degrees for
295 proper focus. The video image is an array of pixels each with 256 levels of
296 light intensity (gray scale). The drop profile is detected using edge-tracing
297 filter routine and the interface is detected using a local threshold and in-
298 terpolation routine. The volume (v) and surface area (A) of the image are
299 calculated using linear interpolation of the drop profile. The temperature of
300 the IFT-chamber is controlled by a Type-J thermocouple fitted with a digi-
301 tal indicator. The pressure of the system is maintained externally through a
302 syringe pump (maximum pressure of 82.7 MPa or 827 bar, Vindum).

303

304 *2.5.3. ST and IFT reduction analyses for brine and heavy crude oil system* 305 *(confined-chamber measurements)*

306 In the current work, heavy crude-brine/SLs system has been taken as the
307 reference fluid with brine or brine/SLs being the environmental phase/fluid
308 and heavy crude the drop phase/fluid. The steps involved in the IFT mea-
309 surement are as follows:

- 310 • The IFT-chamber is filled with the environmental fluid at a set pressure
311 and injection rate of $0.01 \text{ dm}^3 \text{ min}^{-1}$ using an accumulator primed by
312 a syringe pump. At all times, the pressure inside the IFT-chamber
313 is maintained and the temperature set and maintained by a Type-J
314 thermocouple connected to a heating controller.

- 315 • Once the IFT-chamber containing the environmental fluid has attained
316 the required pressure and temperature, a pendant drop of the the refer-
317 ence fluid (crude oil) is gradually created at a very low injection rate of

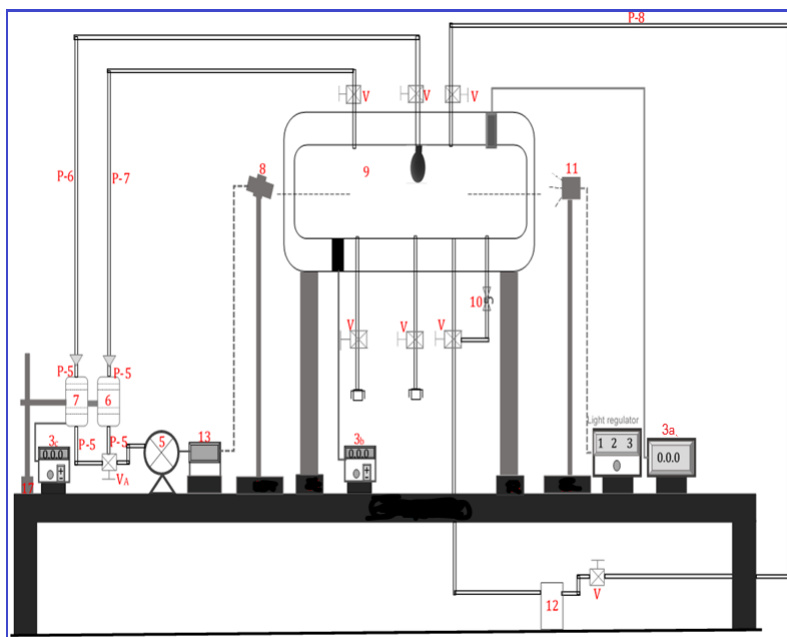


Figure 5: Schematics of the developed HPHT IFT experimental set-up showing: tubing pipes (P5-P8); valves (V); digital indicators and regulators (items 3a, 3b and 3c); syringe pump (item 5); accumulators (items 6 and 7); video-camera (item 8); HPHT IFT-chamber (item 9); pressure relief valve device (item 10); illuminator (item 11); effluent tank (item 12); data acquisition system (item 13).

318 $0.00002 \text{ dm}^3 \text{ min}^{-1}$ through a customised capillary drop needle system
 319 and regulated using a two-way stainless steel valve.

- 320 • As soon as the pendant drop is created, the camera and the DROP
 321 image software starts to capture the high-resolution digital images of
 322 the pendant drop for analysis.
- 323 • The density data of the reference fluid and density of environmental
 324 fluid were used as an input to the software to obtain the dynamic and
 325 equilibrium IFT of the heavy-crude/brine/SLs system.
- 326 • The fundamental principle involved in the calculation of IFT from the
 327 aforementioned measurement procedure is described below.

328 *2.5.4. Specific conductance measurements*

329 The specific conductances for the SLs in distilled water were measured
 330 by using a digital conductivity/TDS metre with a dip type conductivity
 331 cell from JENWAY, UK. It has an automatic temperature compensation of
 332 1.91% per °C. In order to eliminate the variation in conductivity readings
 333 with temperature the samples were maintained at the reference temperature
 334 by using an equivalent of a thermostatic water bath. Before starting the
 335 measurements, the conductivity metre was calibrated by using a KCl solution
 336 of known conductivity as reference and the system equilibrated at an average
 337 temperature of 25°C for at least 30 min.

338 *2.6. Surface excess and thermodynamics of adsorption - brine-SLs*

339 The concentration of SLs molecules in the surface plane relative to bulk
 340 phase (i.e. brine-SLs surface excess) is measured and used to analyse the
 341 behaviour of biosurfactants at the interface by Gibbs adsorption equation.
 342 From the concentration and surface tension data, the surface excess con-
 343 centration (Γ_{min}) of SLs at their critical micelle concentration (CMC) was
 344 determined. The general form of the Gibbs (Gibbs [33]) equation for a system
 345 at constant temperature can be written as:

$$d\gamma = - \sum_i \Gamma_i^\sigma d\mu_i \quad (7)$$

346 where, Γ_i^σ is the surface excess concentration of component i , γ is the
 347 ST or IFT, R is the universal gas constant, T is the temperature, μ_i is the
 348 chemical potential of component i which can be expressed as:

$$\mu_i = \mu_i^o + RT \ln a_i. \quad (8)$$

349 Differentiating equation 8 under constant temperature gives:

$$d\mu_i = RT d \ln a_i. \quad (9)$$

350 μ_i^o is the standard chemical potential of component i . Applying equa-
 351 tion 9 to equation 7 gives the common form of the Gibbs equation for non-
 352 dissociating systems (e.g., non-ionic biosurfactants), thus:

$$d\gamma = -\Gamma_2^\sigma RT d \ln a_2, \quad (10)$$

353 which can also be written as:

$$\Gamma_2^\sigma = -\frac{1}{RT} \frac{d\gamma}{d \ln a_2}, \quad (11)$$

354 In the presence of dissociating solute, such as anionic surfactants of the
 355 form A^-B^+ and assuming ideal behaviour below the CMC, equation 10 be-
 356 comes

$$d\gamma = -\Gamma_A^\sigma d\mu_A - \Gamma_B^\sigma d\mu_B, \quad (12)$$

357 If no electrolyte is present, electroneutrality of the interface will mean
 358 that $\Gamma_A = \Gamma_B$ and the Gibbs equation for a 1 : 1 dissociating compounds can
 359 be written as:

$$\Gamma_2^\sigma = -\frac{1}{2RT} \frac{d\gamma}{d \ln a_2}, \quad (13)$$

360 The following relations are then used to determine the minimum area per
 361 molecule of surfactant (A_{min}) and the free energy of micellisation per mole
 362 of a fully ionised SL surfactant.

$$A_{min} = \frac{10^{16}}{N_A \Gamma_{min}}, \quad (14)$$

$$\Delta G_m^0 = (1 + \alpha)RT \ln X_{cmc}, \quad (15)$$

363 where,

$$\alpha = (1 - \beta), \quad (16)$$

$$\beta = \frac{S_2}{S_1}, \quad (17)$$

364 α is the degree of counter-ion dissociation, X_{cmc} is the CMC of SLs bio-
 365 surfactant in terms of its mole fraction in aqueous solution, β is degree of
 366 ionisation, S_1 and S_2 are the slopes of conductivity versus concentration plot
 367 for the pre- and post-micellar region respectively, ΔG_m^0 is the change in Gibbs
 368 free energy estimated at the CMC (KJmol^{-1}), R is the gas constant (8.314
 369 $\text{J K}^{-1} \text{mol}^{-1}$), a is the activity which can be replaced by concentration c
 370 without loss of generality, N_A is the Avogadro's number ($= 6.022 \times 10^{23} \text{mol}$
 371 $^{-1}$), T is the temperature (298.15K or 25°C , 318.15K or 45°C and 338.15
 372 K or 65°C), and n is the sum of charge number of all ions resulted from the

373 ionisation of the surfactant molecule (i.e. $n= 1$ for non-ionic surfactants and
374 $n= 2$ or 3 for mono or divalent counter ion, respectively).

375 3. Results and discussion

376 3.1. Anaerobic cultivation of *Meyerozyma* spp. MF138126 under ambient 377 conditions

378 *Meyerozyma* spp. MF138126 was incubated under anaerobic ambient
379 conditions. Fig. 6 shows the results of a typical growth curve post-incubation
380 of one week. The yeast strain showed considerable growth as significant
381 turbidity in the culture medium was observed even after 48 h of inoculation.
382 It was noted that *Meyerozyma* spp. MF138126 harboured a lag phase of 48 h
383 which was followed by a log phase of 96 h. Afterwards, a constant stationary
384 phase was recorded during which no apparent increase in microbial growth
385 was observed.

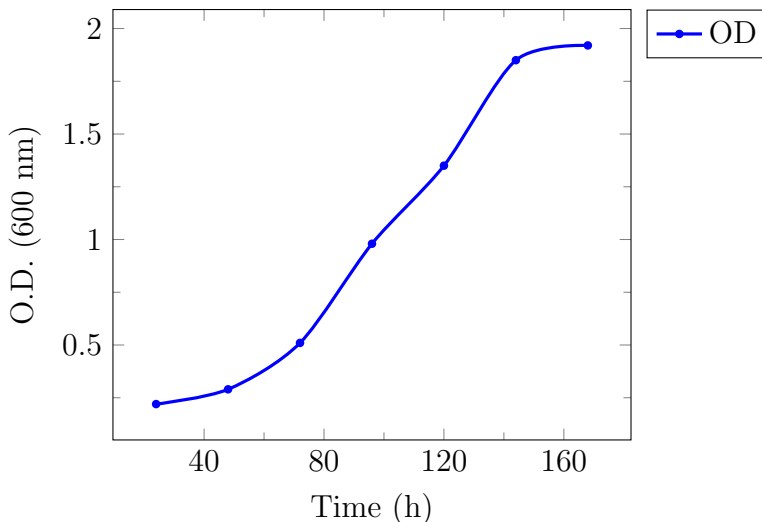


Figure 6: Growth curve - optical density (O.D.) measurement versus time - for *Meyerozyma* spp. MF138126 during incubation under anaerobic ambient conditions.

386 3.2. Anaerobic cultivation of *Meyerozyma* spp. MF138126 under HPHT con- 387 ditions

388 *Meyerozyma* spp. MF138126 was subjected to different anaerobic HPHT
389 conditions in the reactor chamber. Fig. 7 shows the results of a typical

390 growth curve post-incubation of one week. Pressures of 1 bar and 10 bar
 391 were imposed on the reactor cell in a sequential experiment under two dif-
 392 ferent temperatures (25 °C and 45 °C). Initially the culture density of 0.1
 393 was recorded which increased considerably to 0.462 at the end of log phase,
 394 despite the increase in temperature from 25 to 45 °C. The biomass produced
 395 under HPHT conditions was comparatively lesser than that obtained in shake
 396 flasks fermentation cultivation conducted under ambient conditions. How-
 397 ever, display of all the three phases of growth by *Meyerozyma* spp. MF138126
 398 even under HPHT conditions showed the effective acclimatisation of the mi-
 399 croorganism to the surrounding adverse environment. Moreover, a notable
 400 increase in cellular biomass even at high temperatures showed that the yeast
 401 strain can be an effective cellular resource for insitu experimental conditions.

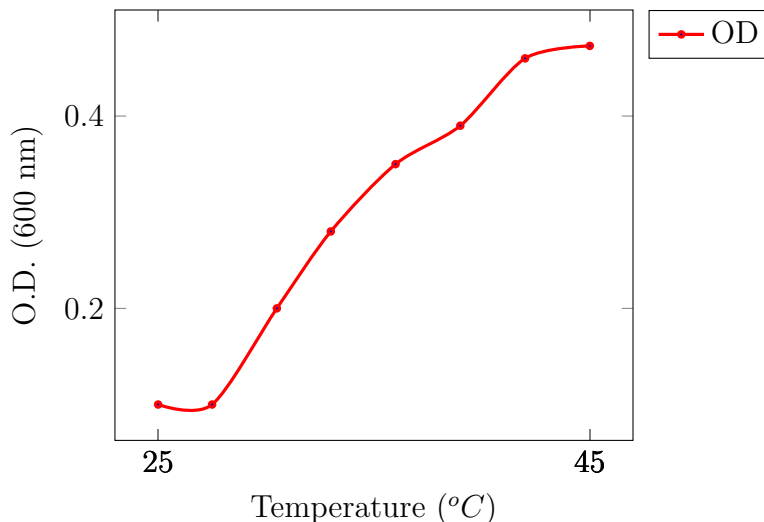


Figure 7: Growth curve - optical density (O.D.) measurement versus temperature - for *Meyerozyma* spp. MF138126 under anaerobic high-pressure high-temperature conditions.

402 **4. Application of SLs produced by *Meyerozyma* spp. MF138126 in** 403 **interfacial phenomena**

404 Surfactants can form oriented interfacial monolayers and aggregate to
 405 form micelles at sufficiently high concentration. The reduction in ST and IFT
 406 is achieved through the adsorption of surfactants micelles at the interface. A

407 number of factors such as surfactant concentration, temperature, pH, salinity
408 etc affect the rate of adsorption of the SLs at the interface. For this particular
409 reason, the ST and IFT reduction was studied in a typical reservoir crude oil-
410 formulation brine mixture for SLs produced by *Meyerozyma* spp. MF138126
411 under varying concentration, pressure, temperature and pH.

412 The supernatant obtained at 25 °C of incubation showed significant re-
413 duction in ST and IFT of the SLS-brine and heavy crude oil mixture at
414 the three aforementioned temperatures of 25, 45 and 65 °C. It was ob-
415 served that the pH of the mixture reduced with increasing concentration of
416 sophorolipids. Similar was the case for ST and IFT. The least ST value
417 of 14 mN/m was observed with the highest concentration of sophorolipids.
418 IFT values when tested under the same temperature conditions showed that
419 with increasing temperature, a continuous decline in brine-crude IFT in the
420 presence of SLs manifests.

421 4.1. FTIR spectroscopic analysis of the SLs produced under HPHT conditions

422 Fig. 8 shows the standard SLs purchased from Sigma Aldrich and Fig.
423 9 shows the FTIR spectrum of crude SLs produced by *Meyerozyma* spp.
424 MF138126 under HPHT conditions. It was noted that most of the peaks
425 lie in the same spectrum for both samples. A broad band observed within
426 the range of 3200-3500 cm^{-1} is due to the characteristic hydroxyl (O-H)
427 stretch whereas, the two bands at 2923 and 2855 cm^{-1} represent the asym-
428 metric and symmetric stretching of methylene groups (CH_2), respectively.
429 The band at 1634 cm^{-1} corresponds to the stretching of unsaturated C=C
430 linkage whereas the band at 1457 cm^{-1} is the C-O-H group in the plane
431 bending of carboxylic moiety in SLs. Moreover, the carbonyl stretch C-O
432 of lactonic SLs was observed at 1046 cm^{-1} . This structural analysis of SLs
433 produced by *Meyerozyma* spp. MF138126 under HPHT conditions is also
434 in accordance with the previous reports of Bajaj and Annapure [34], El-
435 Sheshtawy et al. [35] and Jiménez-Peñalver et al. [36].

436
437 The current findings suggest that the produced SLs is not only effec-
438 tive under ambient conditions but also under HPHT in unconfined systems.
439 Moreover, the molecular integrity of SLs was retained even at this elevated
440 conditions considered to be a harsh environment.

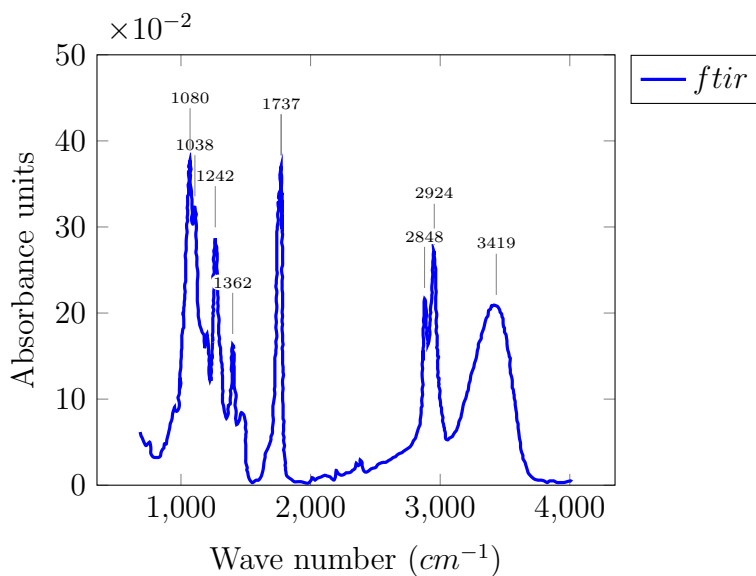


Figure 8: FTIR spectrum of standard sophorolipids.

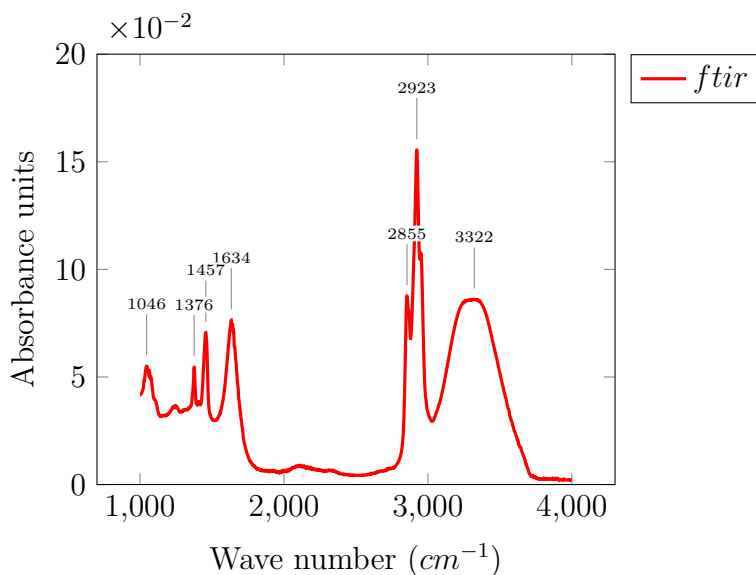


Figure 9: FTIR spectrum of sophorolipids produced by *Meyerozyma* spp. MF138126 under HPHT conditions.

441 *4.2. ST and IFT reduction analyses*

442 The results of the unconfined and confined-chamber measurements are
 443 presented in this section. Table 3 shows the summary of the material prop-

444 erties associated with ST and IFT measurements for the unconfined and
 445 confined-chamber experiments.

446

Table 3: Description of material properties

Drop phase	Heavy crude oil
Environmental phase	Brine + SLs (biosurfactant)
Crude density, ρ_d (g-cm ⁻³)	0.9985
Crude total acid number, TAN (mg KOH/g)	3.7
Crude total base number, TBN (mg KOH/g)	5.0
Asphaltene content (% m/m)	3.6
Brine + SLs density, ρ_e (g-cm ⁻³)	1.027
Molecular weight of SLs (g-mol ⁻¹)	711
Acceleration due to gravity (m-s ⁻²)	9.81
Stock brine concentration (mg/L)	0.50958

447 *4.2.1. ST and IFT reduction analyses for unconfined measurements*

448 Figs. 10 and 11 show the effect of SLs concentration on ST and IFT of the
 449 crude oil-brine system. For this purpose, 2-20 vol. % concentrated solutions
 450 of SLs were prepared. Initially, the ST of brine-SLs mixture was recorded
 451 then IFT of the crude oil-brine/SLs systems. It was observed that with an
 452 increase in concentration, the ST of brine solution decreased continuously
 453 till 12 vol. % (0.17 mM) concentration of SLs. After this point, a constant
 454 ST value of 14 mN/m was recorded which remained constant up to 20 vol.
 455 % (0.28 mM) concentration of SLs in brine formulation. Similarly, a linear
 456 increase in SLs concentrations resulted in reduction of IFT for crude oil-SLs-
 457 brine system. The IFT value decreased from 25 mN/m to 11 mN/m at 12
 458 % SLs concentration and 25 °C, after which it remained almost constant.
 459 However, with similar concentration, the IFT value further decreased up to
 460 the point of 3 mN/m and 0.5 mN/m when the temperature was elevated to
 461 45 °C and 65 °C, respectively. The mean, standard deviation and standard
 462 error of all the measurements are stated in Tables SA.1 - SB.2 (Appendix A
 463 - Appendix B) . This result demonstrates, for the very first time, that SLs
 464 not only significantly reduced the ST and IFT of the COBBIO system but
 465 that it does so at a very low concentration of 12 vol. % (0.17 mM).

466

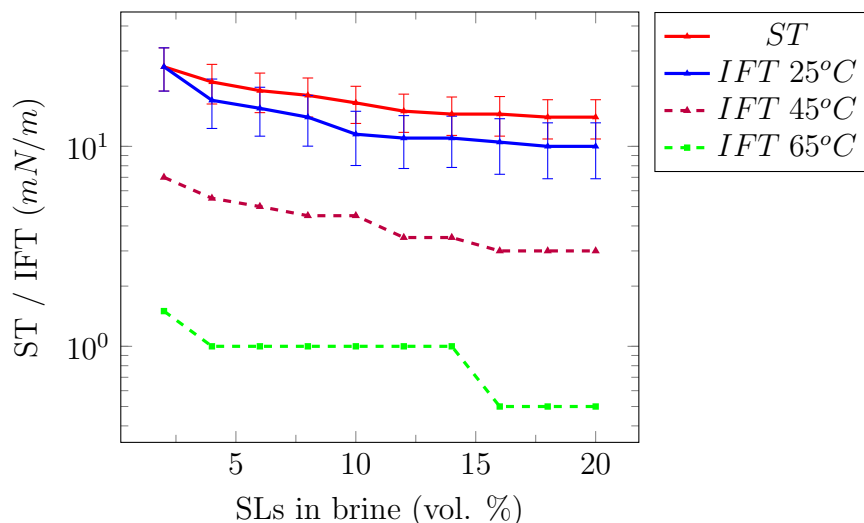


Figure 10: Equilibrium ST and IFT for sophrolipids produced from *Meyerozyma* spp. MF138126 at 25°C. The experiments were carried out using the aqueous solution of SLs in brine with heavy crude-oil at different temperatures.

467 *4.2.2. ST and IFT reduction analyses for confined-chamber measurements*

468 For the confined-chamber measurements, each experimental run was re-
 469 peated at least three times under a fixed pressure and temperature with ten
 470 computational points generated for all the constitutive variables highlighted
 471 in section 2.4. Tables SD.4 - SD.14 of Appendix D show the results of the
 472 data generated for the HPHT IFT measurements between the environmen-
 473 tal phase (brine plus SLs) and the drop-phase (heavy crude-oil) at different
 474 pressures of 1 to 80 bar and fixed temperature of 25°C.

475
 476 In order to validate the obtained dataset, analytical calculations were
 477 carried-out for the IFT values (γ_c) and compared with those obtained from
 478 the DROPImage software (γ_s). Figs. 12 - 13 show the validation results for
 479 the IFT versus time at pressures of 1 and 25 bar. Both values (γ_c and γ_s)
 480 were exactly the same for almost all the 10 points generated for each run
 481 at equilibrium; with a minimum and maximum error of 0.02% and 0.52%
 482 for 1 bar and 0.01% and 0.41% for 25 bar respectively. Similar profile was
 483 obtained in all the repeat-runs (Figs. 12 - 13).

484
 485 Biosurfactants produced by isolated microorganisms have been reported

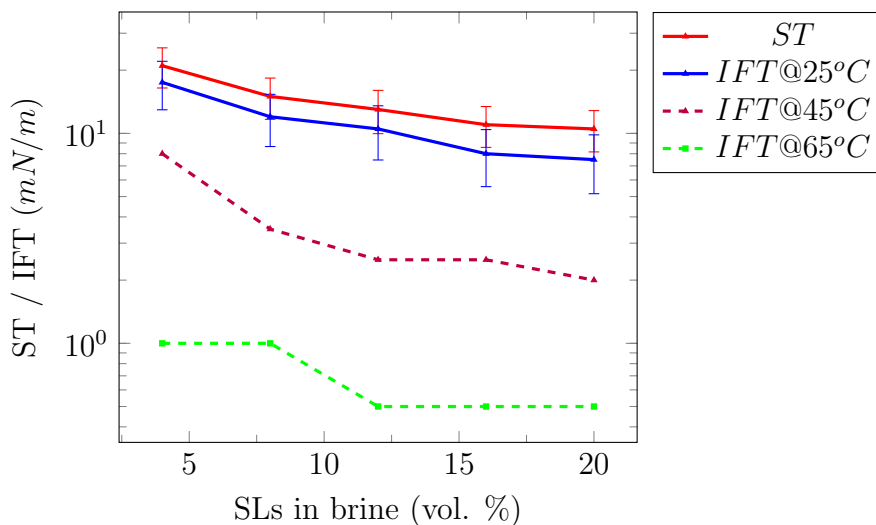


Figure 11: Equilibrium ST and IFT for sphingolipids produced from *Meyerozyma* spp. MF138126 at 45°C. The experiments were carried out using the aqueous solution of SLs in brine with heavy crude-oil at different temperatures.

486 to reduce the IFT between oil and water to 10 mNm^{-1} (Parkinson [37]) or
 487 values slightly less than 10 mNm^{-1} for improved oil recovery process (McIn-
 488 erney et al. [38]); albeit, under unconfined low-pressure conditions. Figure
 489 14 shows the variation of IFT as a function of pressure at a fixed temper-
 490 ature of 25°C in a confined-chamber system. Under confinement, the IFT
 491 of the COBBIO system (heavy crude oil/brine/SLs aqueous) at a pressure
 492 of 1 bar was 4.27 mN/m ; reducing significantly to 0.251 mN/m when the
 493 pressure was gradually increased to 45 bar at the same temperature of 25°C.
 494 Increase in pressure basically caused the molecules of SLs to become more
 495 active in breaking the binding force between the crude oil and the brine,
 496 thereby, accelerating the rate of IFT reduction. The IFT value obtained at
 497 1 bar under confined-chamber experiment (i.e. 4.27 mN/m) is significantly
 498 lower when compared with the value obtained under unconfined measure-
 499 ments (i.e. 25 mN/m) at the same temperature of 25°C; despite the fact
 500 that the concentration was more than three orders of magnitude less in the
 501 confined experiments. This suggests that the effectiveness of SLs in reducing
 502 IFT is amplified under elevated or insitu pressure; making SLs a promising
 503 biosurfactant for EOR projects. Economic viability of SLs in EOR appli-
 504 cations will be evaluated as part of separate investigation involving crude

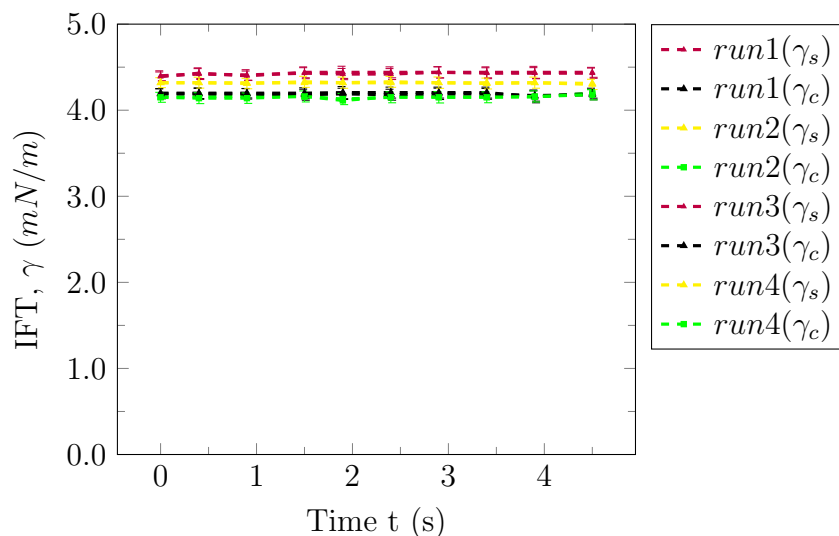


Figure 12: Validation results for a typical confined-chamber IFT experiments conducted at a pressure of 1 bar and temperature of 25°C. γ_c is the IFT values obtained from analytical calculations and γ_s is the DROImage IFT values.

505 oil/brine/biosurfactant/rock (COBBIOR) system.

506 4.3. Effect of temperature on IFT of the system

507 IFT reduction studies were conducted at 25, 45 and 65 °C using different
 508 concentrations of SLs produced by *Meyerozyma* spp. MF138126. In the
 509 first set of experiments, the supernatant obtained from microbial culture
 510 incubated at 25 °C was used and IFT values ranging between 0.5 and 25
 511 mN/m were recorded. Figs. 10 and 11 show a significant decline in IFT of
 512 SLS-brine and crude oil with temperature. Elevated temperature enhances
 513 the solubility of solvents and favours the formation of water-in-oil emulsions
 514 rather than oil-in-water emulsions (Ye et al. [39]). This inversion of phases
 515 facilitates the adsorption of surfactant monomers and eventually reduction
 516 of IFT. Mirchi et al. [40] stated that high temperature increases the kinetic
 517 energy and reduces the attractive forces between molecules. This also causes
 518 a decrease in IFT of the solution and oil.

519 4.4. Effect of pH on IFT of the system

520 pH of the brine-SLs mixture was monitored with varying biosurfactants
 521 concentration. Results (Fig. 15) shows a decrease in pH from 7.8 to 6.78 at

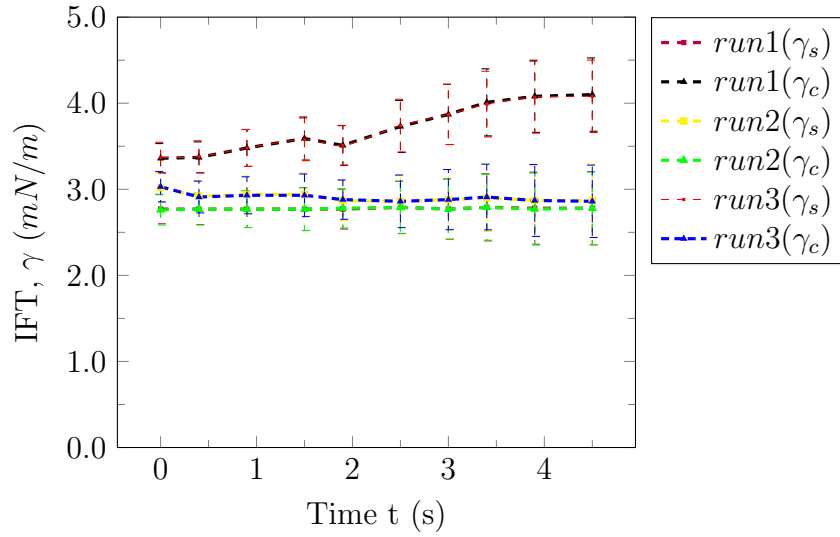


Figure 13: Validation results for a typical confined-chamber IFT experiments conducted at a pressure of 25 bar and temperature of 25°C. γ_c is the IFT values obtained from analytical calculations and γ_s is the DROImage IFT values.

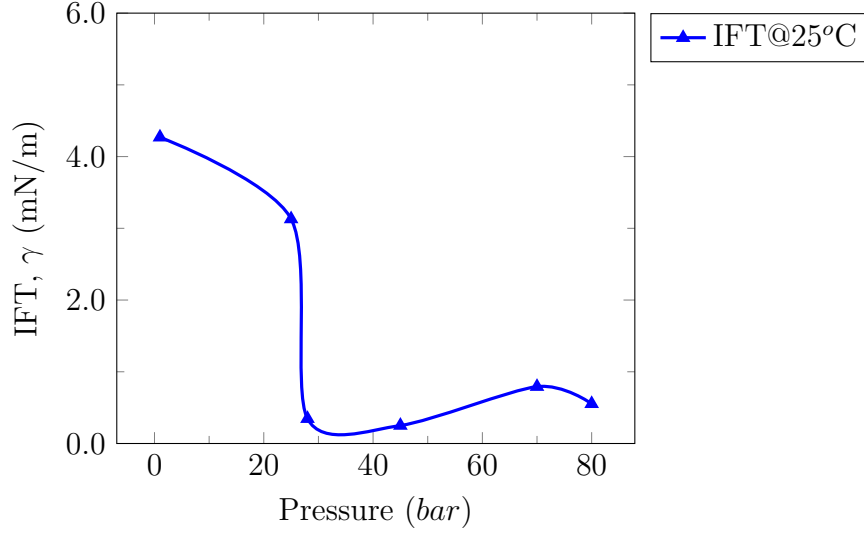


Figure 14: Equilibrium IFT for brine/SLs - heavy crude systems at a fixed temperature of 25°C and pressures of 1 - 80 bar

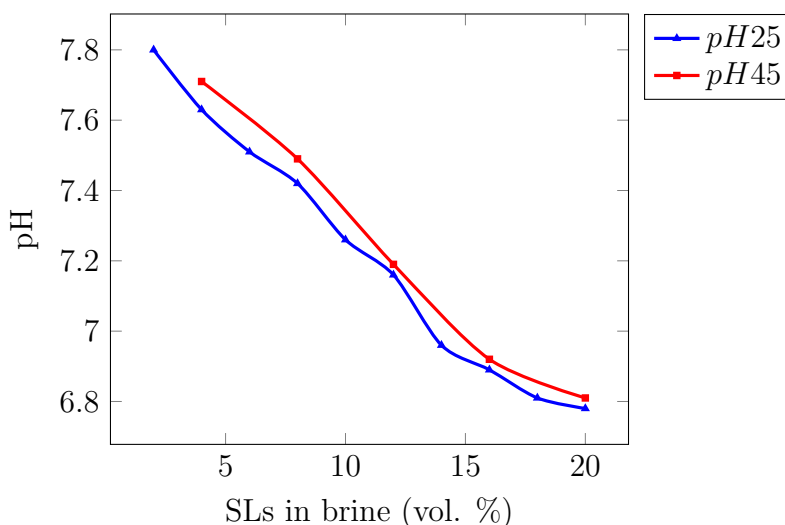


Figure 15: pH as a function of sophorolipids concentration for anaerobic microbial fermentation at 25°C and 45°C respectively.

522 25°C anaerobic fermentation when the SLs concentration was increased from
 523 2% to 20 %; and from 7.71 to 6.81 at 45°C anaerobic fermentation when the
 524 SLs concentration was increased from 2% to 20 %, respectively. The impact
 525 of fermentation temperature on the system pH is also observed as part of
 526 this analysis (see Fig. 15). pH plays a very important role in surfactants
 527 adsorption on liquid-liquid and liquid-rock surfaces for anionic surfactants.

528 4.5. Analysis of thermodynamic properties

529 Figs. 18 - 23 show graphs of surface excess concentration Γ (mol/m^2)
 530 versus the change in $\ln c$ (i.e. $d \ln c$) for different values of γ (i.e. $d\gamma$).
 531 Both cases of ST and IFT measurements at 25°C, 45°C, 65°C and microbial
 532 fermentation of both 25°C and 45°C, were investigated respectively.

533
 534 The surface excess concentration, Γ provides a direct information about
 535 the interaction of the molecules of SLs and the other phases at an interface
 536 when a brine is enriched at that interface. The observed reduction in surface
 537 tension when the solution concentration is increased indicates that SLs is a
 538 surface active agent. The analysis conducted in this study further revealed
 539 the fact that the Γ not only reduced with increase in change in $\ln c$ (i.e.
 540 $d \ln c$), but, the profile of the plots changes depending on the values of γ

Table 4: Minimum area per molecule of sophorolipids biosurfactant A_{min} (cm^2) at different measurement and anaerobic fermentation temperatures.

	ST	IFT		
	$25^\circ C$	$25^\circ C$	$45^\circ C$	$65^\circ C$
$25^\circ C$ anaerobic fermentation	1.43E-05	7.13E-06	3.80E-05	0.00011
$45^\circ C$ anaerobic fermentation	9.50E-06	3.80E-05	1.27E-05	0.00011

541 (i.e. $d\gamma$) which is also implicitly dependent on concentration. This can be
 542 seen in a typical graphical plot (e.g. Fig. 18). The effect of temperature
 543 on the surface excess concentration can also be seen in Figs. 18 - 20 for
 544 the microbial fermentation temperature of $25^\circ C$ and Figs. 21 - 23 for the
 545 microbial fermentation temperature of $45^\circ C$. As the temperature increases,
 546 the degree of SLs adsorption at the interface increases leading to a collapse
 547 in the trends of the Γ . Table 4 indicates the minimum area per molecule of
 548 SLs for the different experimental and cultivation temperatures investigated
 549 in this study. It shows that when SLs was added, the interface weakens
 550 occupying more surface area as the temperature increases. This observation
 551 is in line with Kosaka et al. [41]. The degree of counter-ion binding for SLs
 552 was obtained to be 0.86. The computed Gibbs free energy of micellisation is -
 553 1940 KJmol^{-1} (i.e. $\Delta G < 0$) which is exergonic depicting favourable reaction
 554 and spontaneous in forward direction. Process reactions are endergonic and
 555 unfavourable when $\Delta G > 0$ and energy is absorbed.

556 4.6. Specific conductance in the bulk

557 The specific conductance, κ , of the different surfactant solutions is plotted
 558 in Fig. 24. Each plot shows that conductivity linearly correlated with the
 559 surfactant concentration in the pre-micellar and post-micellar regions. The
 560 intersection between two straight lines gives the break point, and hence cmc
 561 value. The cmc values obtained from κ measurements is $3.703 \times 10^{-3} \text{ mol/L}$.

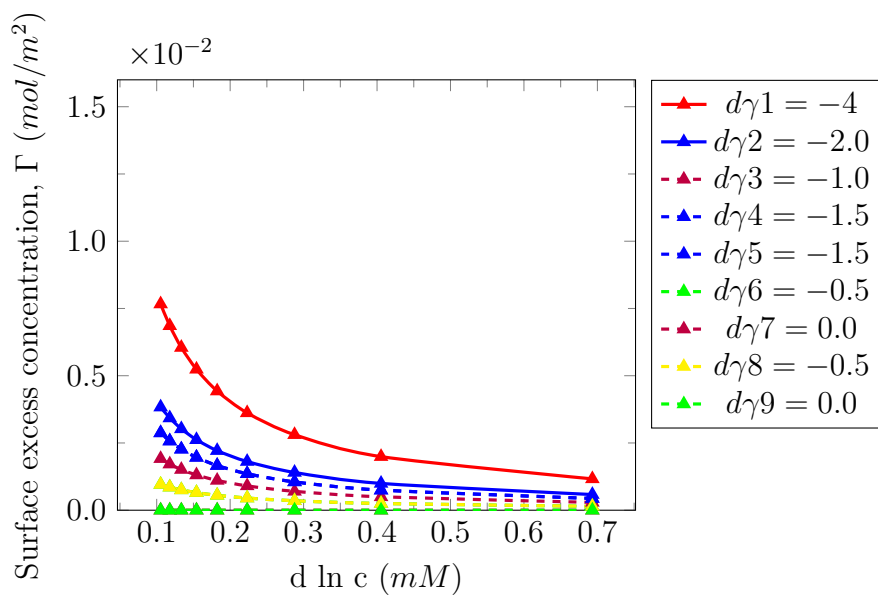


Figure 16: Surface excess concentration (mol/m^2) versus $d \ln c$ for different values of $d\gamma$ - ST measurements at 25°C and microbial fermentation at 25°C .

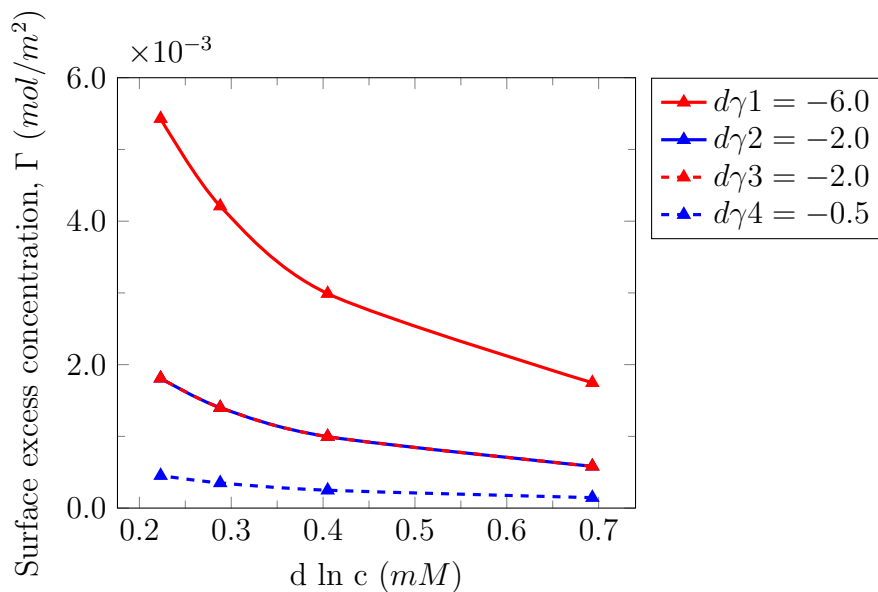


Figure 17: Surface excess concentration (mol/m^2) versus $d \ln c$ for different values of $d\gamma$ - ST measurements at 25°C and microbial fermentation at 45°C .

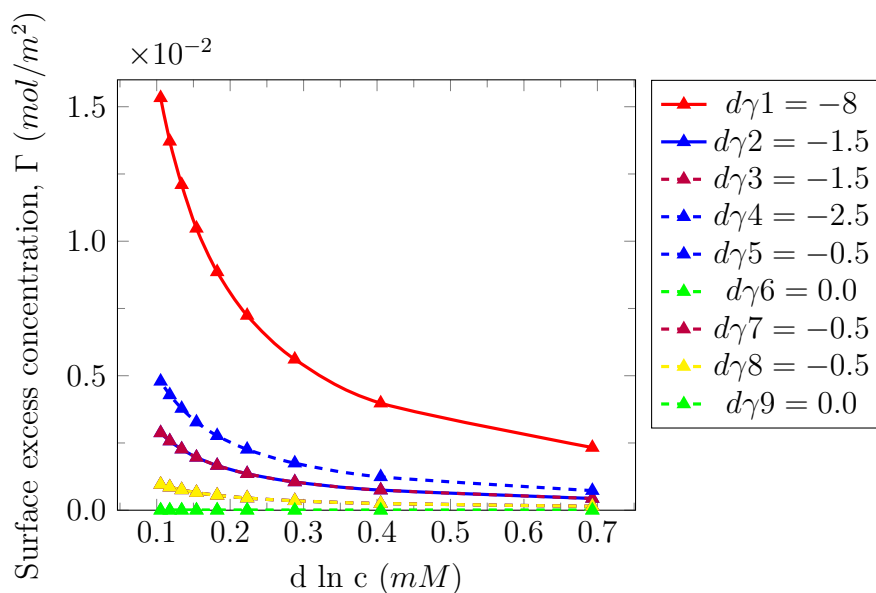


Figure 18: Surface excess concentration (mol/m^2) versus $d \ln c$ for different values of $d\gamma$ - IFT measurements at $25^\circ C$ and microbial fermentation at $25^\circ C$.

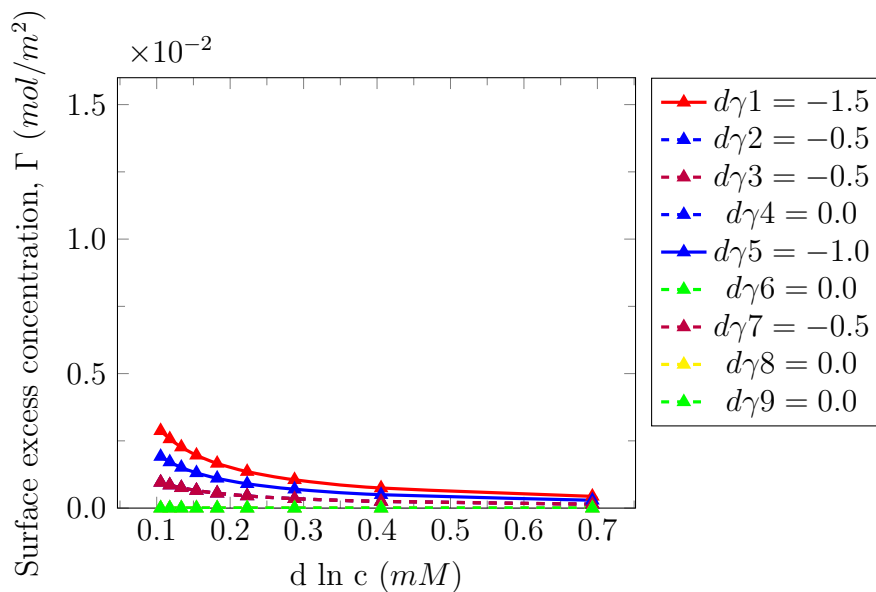


Figure 19: Surface excess concentration (mol/m^2) versus $d \ln c$ for different values of $d\gamma$ - IFT measurements at $45^\circ C$ and microbial fermentation at $25^\circ C$.

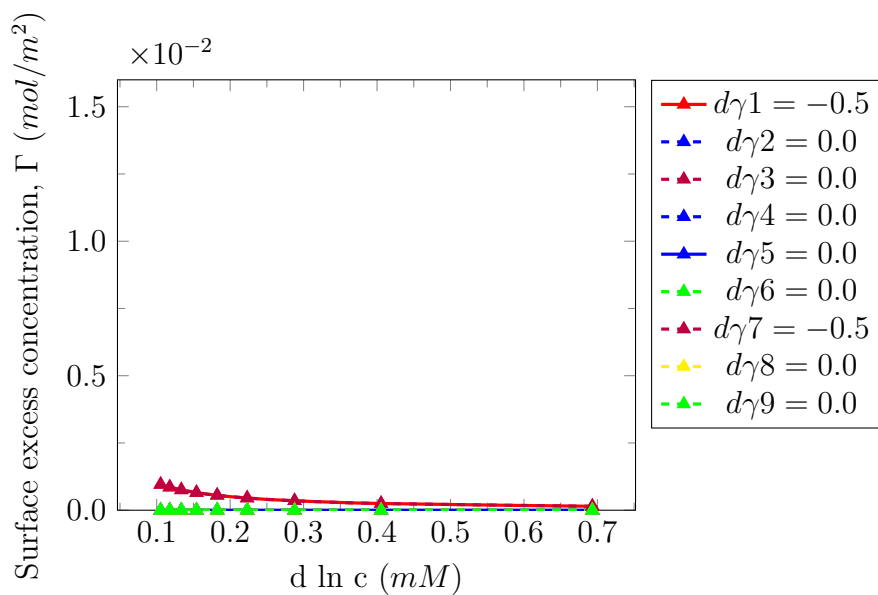


Figure 20: Surface excess concentration (mol/m^2) versus $d \ln c$ for different values of $d\gamma$ - IFT measurements at $65^\circ C$ and microbial fermentation at $25^\circ C$.

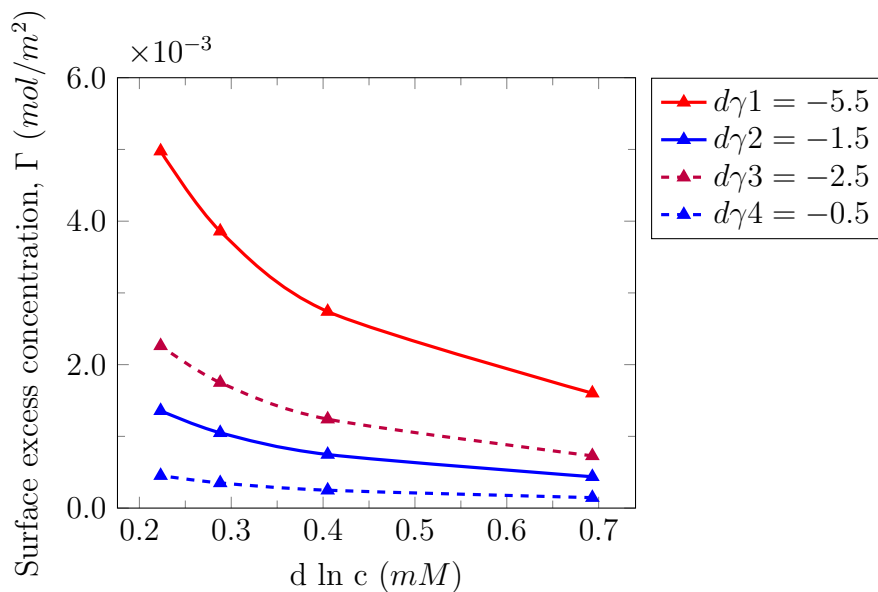


Figure 21: Surface excess concentration (mol/m^2) versus $d \ln c$ for different values of $d\gamma$ - IFT measurements at $25^\circ C$ and microbial fermentation at $45^\circ C$.

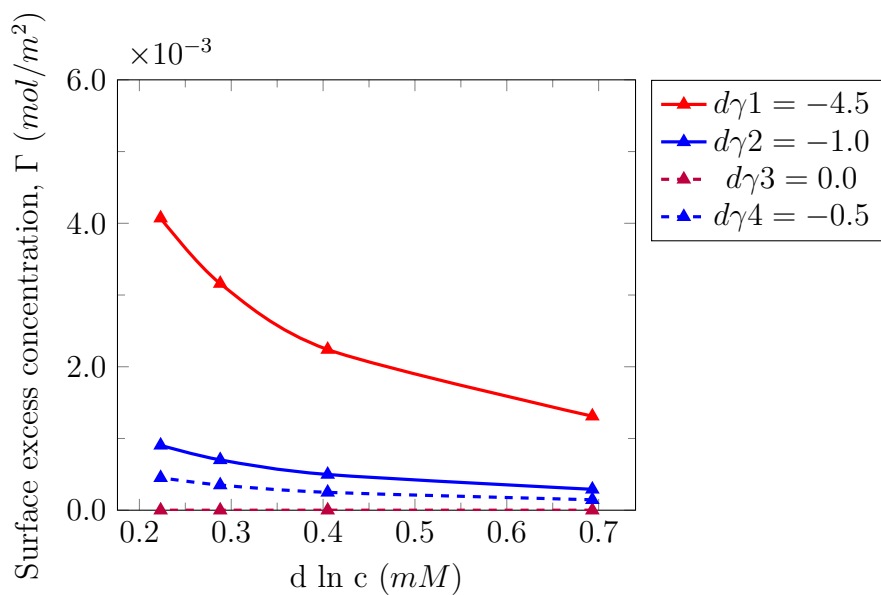


Figure 22: Surface excess concentration (mol/m^2) versus $d \ln c$ for different values of $d\gamma$ - IFT measurements at $45^\circ C$ and microbial fermentation at $45^\circ C$.

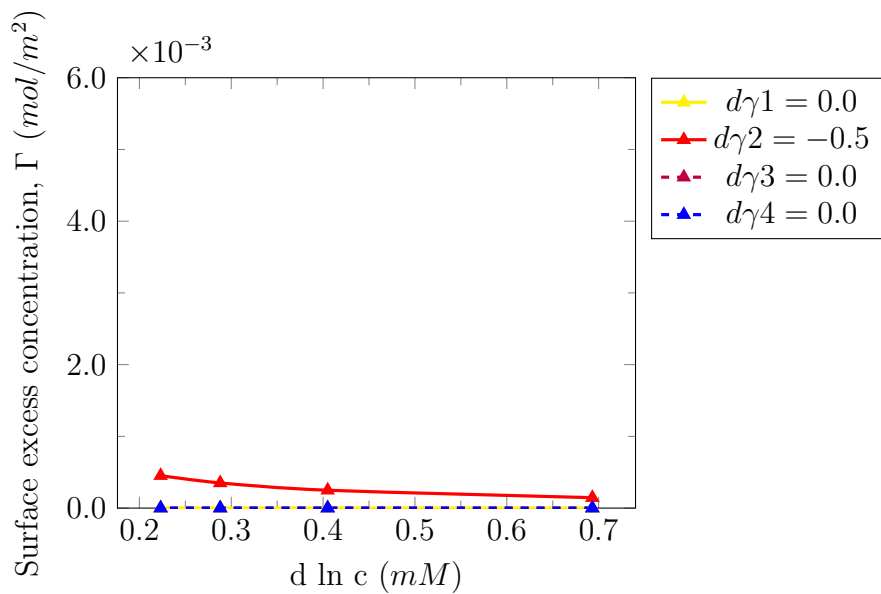


Figure 23: Surface excess concentration (mol/m^2) versus $d \ln c$ for different values of $d\gamma$ - IFT measurements at $65^\circ C$ and microbial fermentation at $45^\circ C$.

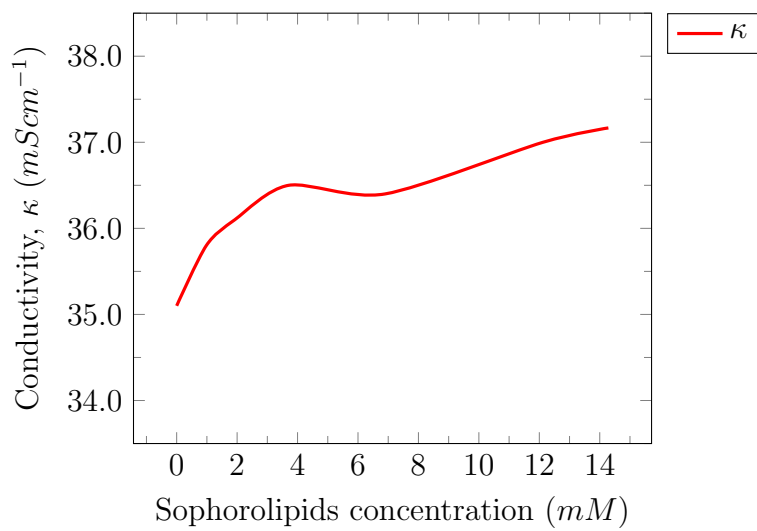


Figure 24: The plot of specific conductivity versus concentration of sophorolipids at 25°C (1 mM = 10⁻³ mol/L).

562 **5. Conclusions**

563 A novel technique for interface behaviour and thermodynamic proper-
564 ties analyses of biosurfactant is developed. The micellisation behaviour and
565 thermodynamic properties of SLs obtained from *Meyerozyma* spp. MF138126
566 under HPHT for low-salinity heavy-crude experiments is studied. The new
567 environmentally benign microbial strain was previously isolated from a crude
568 oil contaminated site and screened for its SLs producing capabilities.

- 569 • A series of anaerobic fermentation experiments under HPHT condi-
570 tions in a reactor chamber is conducted. Samples are collected periodi-
571 cally under varying conditions of temperature and pressure to monitor
572 growth-rate and produced cellular biomass using spectrophotometer.

- 573 • We report for the very first time, the potential of the isolated strain and
574 the produced SLs to reduce IFT between the formulated low salinity
575 formation brine and heavy crude by up to a factor of five (5) and
576 seven (7) for the anaerobic cultivation of $25^{\circ}C$ and $45^{\circ}C$ respectively.
577 Increasing experimental temperature to $45^{\circ}C$ and $65^{\circ}C$ brings about a
578 reduction of a factor of seven (7) and nine (9) in IFT respectively.

- 579 • From the ST results, it can further be concluded that the packing of
580 SLs monomers at brine/SLs and SLs/crude oil interfaces becomes loose
581 at high temperature.

- 582 • Furthermore, using surface tensiometry, the CMC, the thermodynamics
583 of adsorption, surface excess concentration and the minimum area occu-
584 pied by surfactant monomers were determined. The degree of counter-
585 ion binding for SLs is obtained to be 0.86. The computed Gibbs free
586 energy of micellisation is -1940 KJ/mol; which is exergonic depicting
587 favourable reaction and spontaneous in forward direction.

- 588 • IFT value of 0.251 mN/m was obtained at an elevated pressure of 45
589 bar. Similarly, keeping the temperature constant at $25^{\circ}C$ and increas-
590 ing the pressure up to 80 bar, the IFT reduces. It is concluded that the
591 produced SLs retained its molecular integrity and effectiveness under
592 unconfined ambient conditions with an amplified activity under HPHT
593 confined systems.

594 **6. Nomenclature**

595 P = pressure, Pa

596 T = temperature, °C

597 ρ = density, g/cm^3

598 M = molecular weight, g/mol

599 g = acceleration due to gravity, m/s^2

600 R_0 = radius of curvature at the drop apex

601 β = shape factor

602 θ = angle, °

603 V = volume, cm^3

604 D = diameter of pendant drop, cm

605 ν = ratio of diameters of a drop

606 H = drop height, cm

607 μ = fluid viscosity, cp

608 B = transformed shape parameter

609 γ = IFT or ST, mN/m

610 Γ = surface excess concentration, mol/m^2

611 κ = conductivity, mS/cm

612 ρ_e = environmental phase density ($g\text{-}cm^{-3}$)

613 ρ_d = drop-phase density ($g\text{-}cm^{-3}$)

614 R = universal gas constant, 8.314 J/K-mol

615 A_{min} = minimum area per molecule of surfactant, cm^2

616 a = activity

617 c = concentration, mol/L

618

619 **Acronyms**

620 IFT = interfacial tension

621 ST = surface tension

622 HPHT = high-pressure high-temperature

623 SLS = sophorolipids

624 OD = optical density

625 COBR = crude oil/brine/rock

626 COBBIO = crude oil/brine/biosurfactant

627 COBBIOR = crude oil/brine/biosurfactant/rock

628 CMC = critical micelle concentration

629 TDS = total dissolved solid

630 mM = milli-Molarity = 1×10^{-3} mol/L

631 **References**

- 632 [1] T. F. Tadros, Wiley-VCH, Weinheim, 2005.
- 633 [2] A. Koh, A. Wong, A. Quinteros, C. Desplat, R. Gross, Influence of
634 sophorolipid structure on interfacial properties of aqueous-arabian light
635 crude and related constituent emulsions., *Journal of the American Oil*
636 *Chemists* 94 (2017) 107–119.
- 637 [3] T. Bollmann, C. Zerhusen, B. Glösen, U. Schörken, Structures and
638 properties of sophorolipids in dependence of microbial strain, lipid sub-
639 strate and post-modification., *Journal of the American Oil Chemists* 56
640 (2019) 367–377.
- 641 [4] X. Wang, R. Lin, R. Gross, Sophorolipid butyl ester: an antimicrobial
642 stabilizer of essential oil-based emulsions and interactions with chitosan
643 and γ -poly (glutamic acid), *ACS Applied Bio Materials* 3 (2020) 5136–
644 5147.
- 645 [5] G. S. Kiran, T. A. Thomas, J. Selvin, B. Sabarathnama, A. P. Lipton,
646 Optimization and characterization of a new lipopeptide biosurfactant
647 produced by marine *brevibacterium aureum* msa13 in solid state culture,
648 *Bioresource Technology* 101 (2010) 2389–2396.
- 649 [6] G. A. R. Ramos, L. T. Akanji, W. Afzal, A novel surfac-
650 tant–polymer/alkaline–surfactant–polymer formulation for enhanced oil
651 recovery (eor) processes, *Energy & Fuels* - (2019) -. doi:.
- 652 [7] J. D. Desai, I. M. Banat, Microbial production of surfactants and their
653 commercial potential, *Microbiology and Molecular Biology Review* 61
654 (1997) 47–64.
- 655 [8] H. Al-Sulaimani, Y. Al-Wahaibi, A. Al-Bahry, S. Elshafie, A. Al-Bemani,
656 S. Joshi, S. Zargari, Optimization and partial characterization of bio-
657 surfactants produced by *bacillus* species and their potential for ex-situ
658 enhanced oil recovery, *Society of Petroleum Engineers*, 2011.
- 659 [9] J. Chisholm, S. Kashikar, R. Knapp, M. McInerney, D. Menzie, Micro-
660 bial enhanced oil recovery: Interfacial tension and gas-induced relative
661 permeability effects., 20481, 1990.

- 662 [10] A. Budiharjo, H. Jeong, D. Wulandari, S. Lee, C. M. Ryu, Complete
663 genome sequence of bacillus altitudinis p-10, a potential bioprotectant
664 against xanthomonas oryzae pv. oryzae, isolated from rice rhizosphere
665 in java, indonesia., *Genome Announcement* 5 (2017).
- 666 [11] K. Poremba, W. Gunkel, S. Lang, F. Wagner, Toxicity testing of syn-
667 thetic and biogenic surfactants on marine microorganisms, *Environmental*
668 *Toxicology and Water Quality* 6 (1991) 157–163. doi:.
- 669 [12] W. Norde, Driving forces for protein adsorption at solid surfaces, *Macro-*
670 *molecular Symposia* 103 (1996) 5–18.
- 671 [13] K. Nakanishi, T. Sakiyama, K. Imamura, On the adsorption of proteins
672 on solid surfaces, a common but very complicated phenomenon., *Journal*
673 *of Bioscience and Bioengineering* 91 (2001) 233–244.
- 674 [14] M. J. Rosen, Adsorption of surface-active agents at interfaces: the elec-
675 trical double layer., third edition ed., 2004.
- 676 [15] Y. Al-Wahaibi, S. Joshi, S. Al-Bahry, A. Elshafie, A. Al-Bemani,
677 B. Shibula, Biosurfactant production by bacillus subtilis b30 and its
678 application in enhancing oil recovery., volume 114, 2014.
- 679 [16] L. Al-Araji, R. Rahman, M. Basri, A. Salleh, Microbial surfactant.,
680 *Asia Pacific Journal of Molecular Biology and Biotechnology* 15 (2007)
681 99–105.
- 682 [17] J. Anitha, P. Jeyanthi, V. and Ganesh, Production and characterization
683 of biosurfactant by bacillus and its applicability in enhanced oil recov-
684 ery., *International Journal of Advanced Research in Biological Sciences.*
685 2 (2015) 716.
- 686 [18] J. G. Speight, Marcel Dekker, Inc., 1991.
- 687 [19] D. Lanier, Heavy oil - a major energy source for the 21st century., *Techn-*
688 *ical Report 039, UNITAR Centre for heavy crude and tar sands, 1998.*
- 689 [20] D. Keomany, E. Asnachinda, Adsorption and adsolubilization of organic
690 solutes using rhamnolipid biosurfactant modified surface., in: *1st En-*
691 *vironment and Natural Resources International Conference, Thailand,*
692 *2014, p. 231–236.*

- 693 [21] F. P. Camargo, A. J. Menezes, P. S. Tonello, A. C. A. Dos Santos, I. C. S.
694 Duarte, Characterization of biosurfactant from yeast using residual soy-
695 bean oil under acidic conditions and their use in metal removal processes,
696 FEMS Microbiology Letters 365 (2018). doi:, fny098.
- 697 [22] F. P. Camargo, P. P. F. D., P. S. Tonello, A. C. A. Dos Santos, I. C. S.
698 Duarte, Bioleaching of toxic metals from sewage sludge by co-inoculation
699 of acidithiobacillus and the biosurfactant-producing yeast meyerozyma
700 guilliermondii, Journal of Environmental Management 211 (2018) 28–
701 35.
- 702 [23] X. Liang, S. R., R. M., Zhao, F., Y. Zhang, S. Han, Y. Zhang, Anaerobic
703 lipopeptide biosurfactant production by an engineered bacterial strain
704 for in situ microbial enhanced oil recovery, Royal society of chemistry 7
705 (2017) 20667–20676.
- 706 [24] Z. Ganji, K. Beheshti-Maal, A. Massah, Z. Emami-Karvani, A novel
707 sophorolipid-producing candida keroseneae gbme-iauf-2 as a potential
708 agent in microbial enhanced oil recovery (meor), FEMS Microbiology
709 Letters 367 (2020).
- 710 [25] A. Elshafie, S. Joshi, Y. Al-Wahaibi, A. Al-Bemani, S. Al-Bahry, D. Al-
711 Maqbali, I. Banat, Sophorolipids production by candida bombicola atcc
712 22214 and its potential application in microbial enhanced oil recovery,
713 FEMS Microbiology Letters 6 (2015) 1324.
- 714 [26] N. Bagalkot, A. Hamouda, O. Isdahl, Dynamic interfacial tension mea-
715 surement method using axisymmetric drop shape analysis, MethodsX 5
716 (2018) 676–683.
- 717 [27] T. Amirianshoja, R. Junin, A. Kamal Idris, O. Rahmani, A comparative
718 study of surfactant adsorption by clay minerals, Journal of Petroleum
719 Science and Engineering 101 (2013) 21–27. doi:.
- 720 [28] A. Barati-Harooni, A. Najafi-Marghmaleki, A. Tatar, A. H. Moham-
721 madi, Experimental and modeling studies on adsorption of a nonionic
722 surfactant on sandstone minerals in enhanced oil recovery process with
723 surfactant flooding, Journal of Molecular Liquids 220 (2016) 1022–1032.

- 724 [29] R. Rehman, M. I. Ali, U. Qureshi, A. Jamal, Characterization of
725 brownfield: Ex-situ detection of hydrocarbon degrading and biosurfac-
726 tants producing microflora, *Pakistani Journal of Agricultural Science*
727 56 (2019) 953–961.
- 728 [30] C. C. Onyemara, L. T. Akanji, R. Ebel, Development of a new high-
729 pressure high-temperature technology for advanced screening of biosur-
730 factants and injection of microbes in porous rocks during low-salinity eor
731 processes., in: *Artificial Intelligence, Big Data and Mobile Technology:
732 Changing the Future of the Energy Industry*, 2019, p. 26. doi:.
- 733 [31] F. K. Hansen, Dropimage advanced - a program for the measure-
734 ment of interfacial tension and contact angles by image analysis,
735 <http://www.ramehart.com/dropimagefinn.htm>, 2006. Accessed: 2020-
736 01-15.
- 737 [32] W. Heller, M.-H. Cheng, B. W. Greene, Surface tension measurements
738 by means of the “microcone tensiometer”, *Journal of Colloid and Inter-
739 face Science* 22 (1966) 179 – 194.
- 740 [33] J. W. Gibbs, *The Collected Works of J. W. Gibbs*, volume I, Longmans,
741 Green, New York, 1931.
- 742 [34] V. Bajaj, U. S. Annapure, Castor oil as secondary carbon source for
743 production of sophorolipids using *starmerella bombicola*, *oleo science*
744 64 (2015) 315–323.
- 745 [35] H. El-Sheshtawy, I. Aiad, M. Osman, A. Abo-ELnasr, A. S. Kobisy, Pro-
746 duction of biosurfactants by *bacillus licheniformis* and *candida albicans*
747 for application in microbial enhanced oil recovery, *Egyptian petroleum*
748 25 (2016) 293–298.
- 749 [36] P. Jiménez-Peñalver, T. Gea, A. Sánchez, X. Font, Production of
750 sophorolipids from winterization oil cake by solid-state fermentation:
751 optimization, monitoring and effect of mixing., *Biochemical engineering*
752 115 (2016) 93–100.
- 753 [37] M. Parkinson, *Biosurfactants*, *Biotechnology* 3 (1985) 65–83.

- 754 [38] M. J. McInerney, M. Javaheri, D. P. Nagle, Properties of the biosurfac-
755 tant produced by bacillus licheniformis strain jf-2, *Journal of Industrial*
756 *Microbiology* 5 (1990) 95–101. doi:.
- 757 [39] Z. Ye, F. Zhang, L. Han, P. Luo, J. Yang, H. Chen, The effect of temper-
758 ature on the interfacial tension between crude oil and gemini surfactant
759 solution., *Colloids and Surfaces: Physicochemical and Engineering As-*
760 *pects* 322 (2008) 138–141.
- 761 [40] V. Mirchi, S. Saraji, L. Goual, M. Piri, Dynamic interfacial tension and
762 wettability of shale in the presence of surfactants at reservoir conditions.,
763 *Fuel* 148 (2015) 127–138.
- 764 [41] O. Kosaka, P. Sehgal, H. Doe, Behavior of cationic surfactants micellar
765 solution solubilizing an endocrine disruptor bisphenol a, *Food Hydro-*
766 *colloids* 22 (2008) 144 – 149. doi:.